Contents list available at CBIORE journal website

International Journal of Renewable Energy Development

Journal homepage: https://ijred.cbiore.id

Research Article

Synergistic co-pyrolysis of *Gracilaria* waste and waste tires: Enhancing bio-oil quality through thermal and chemical bond optimization

Imron Masfuri[a,b], Shaza Eva Mohamad[a*], Dhani Avianto Sugeng[b], Apip Amrullah[c], Wira Jazair Yahya[a]

[a]*Malaysia-Japan International Institute of Technology, Universiti Teknologi Malaysia Jalan Sultan Yahya Petra 54100 Kuala Lumpur, Malaysia*

[b]*Research Center for Energy Conversion and Conservation, National Research and Innovation Agency, PUSPIPTEK, South Tangerang 15314, Indonesia*

[c]*Department of Mechanical Engineering, Lambung Mangkurat University, Banjarmasin, South Kalimantan, Indonesia*

Abstract. The increasing demand for renewable energy and sustainable waste management has prompted research into innovative conversion technologies. This study explored the co-pyrolysis of Gracilaria waste (GW) and waste tires (WT) as a potential approach to improving bio-oil quality by enhancing its hydrocarbon content and reducing oxygenated compounds. The novelty of this study lay in providing new mechanistic insights into the co-pyrolysis process by systematically analyzing the thermal degradation behavior and chemical bond evolution of GW-WT mixtures using a combination of TGA, FTIR, and GC-MS techniques. This detailed chemical transformation analysis differentiated the study from prior research that primarily focused on product yields. The study analyzed the thermal degradation behavior and chemical bond transformation of GW and WT mixtures during pyrolysis, hypothesizing that the addition of WT to GW would enhance the hydrocarbon profile and thermal stability of the resulting bio-oil. Thermogravimetric analysis (TGA) was employed to evaluate the decomposition behavior of five different GW-WT blend ratios under an inert atmosphere, while Fourier Transform Infrared Spectrosco py (FTIR) was used to assess chemical functional group evolution in both raw materials and pyrolytic products. The results revealed that GW pyrolysis exhibited a single weight loss peak (100–350°C) with a total weight loss of 40%, while WT pyrolysis followed a two-stage decomposition process (200–500°C) with a total weight loss of 65%. The GW-WT mixture resulted in a total weight loss of approximately 60%, indicating a synergistic effect between the two feedstocks. FTIR analysis confirmed a reduction in hydroxyl (-OH) groups and an increase in hydrocarbon-related bonds (C=C, C-C, and C-H), demonstrating improved bio-oil composition. These findings suggested that incorporating waste tires into Gracilaria pyrolysis enhanced bio-oil quality and hydrocarbon content, offering a promising approach for biomass valorization and sustainable energy production. Future research should explore process optimization through catalyst integration and scale-up potential for industrial applications.

Keywords: co-pyrolysis, Gracilaria waste, waste tires, thermal degradation, chemical bonds shift

Received:14th March 2025; Revised: 17th May 2025; Accepted: 24th June 2025; Available online: 18th July 2025

1. Introduction

The escalating global energy demand, driven by industrialization and population growth, necessitates the transition from fossil fuels to more sustainable energy sources. Fossil fuel dependence contributes significantly to greenhouse gas emissions, exacerbating environmental concerns such as global warming and climate change. Additionally, the depletion of conventional energy reserves highlights the urgency of adopting renewable alternatives. Biomass has emerged as a promising renewable energy source due to its carbon-neutral nature and widespread availability. Among various biomass sources, marine-derived biomass waste, particularly the byproducts of the agar industry, presents a viable feedstock for energy production. Gracilaria, a red seaweed abundantly found in Indonesian waters and commonly used for agar production, can be converted into valuable biofuels through thermochemical processes such as pyrolysis (Amrullah *et al.*, 2023; Farobie *et al.*, 2024).

Pyrolysis, a thermochemical decomposition process under inert conditions, has gained attention for converting biomass into liquid bio-oil, gaseous fuels, and solid char (Ma *et al.*, 2023). This process plays a crucial role in sustainable waste management while providing a renewable energy source (Chen *et al.*, 2023; Prasetiawan *et al.*, 2024)). Additionally, bio-oil derived from pyrolysis, commonly referred to as pyrolytic oil or bio-crude oil, is a complex mixture of organic compounds with potential applications in energy and chemical industries (Masfuri *et al.*, 2024). Solid waste management is another critical challenge, particularly concerning the disposal of waste tires, which accumulate in massive quantities, with approximately 300 million discarded annually worldwide (Li *et al.*, 2023). As a

* Corresponding author
Email: shaza@utm.my (S. E. Mohamad)

https://doi.org/10.61435/ijred.2025.61202
ISSN: 2252-4940/© 2025.The Author(s). Published by CBIORE

carbonaceous solid waste, waste tires possess high energy content and hydrocarbon composition, making them a promising feedstock for pyrolysis (Mavukwana *et al*., 2021). Conventional landfill disposal poses severe environmental risks, necessitating the development of environmentally friendly disposal techniques (Wang *et al*., 2023b). Pyrolysis of waste tires offers an efficient solution by transforming them into valuable energy products while mitigating environmental pollution (Alzahrani *et al*., 2025; F. Wang *et al*., 2022). The co-pyrolysis of biomass with plastic waste, such as polyethylene terephthalate (PET), has been studied to enhance bio-oil yield and improve fuel quality (Amrullah *et al*., 2024).

Given their high carbon content and energy potential, waste tires have been identified as an effective co-pyrolytic reactant when combined with biomass. Co-pyrolysis, which involves the simultaneous thermal degradation of multiple feedstocks, enhances the quality of pyrolysis products due to synergistic interactions (Abnisa & Wan Daud, 2014). Researchers have demonstrated that co-pyrolysis improves the yield and quality of bio-oil by optimizing the hydrogen-to-carbon ratio (Zhang *et al*., 2024). Waste tires and biomass co-pyrolysis has been investigated with various feedstocks, including wood biomass and polyethylene, with results indicating improved liquid fuel production (Hussain *et al*., 2021; Martínez *et al*., 2014b). The interaction between biomass and rubber-derived compounds further contributes to the complexity and diversity of the pyrolysis liquid, which contains a range of valuable chemicals such as acids, ketones, phenols, and aromatics (González *et al*., 2010; Kim, 2015). The thermochemical conversion of macroalgae such as *Ulva lactuca*, *Padina sp.* has also been explored, with studies showing the potential of marine biomass for producing biofuels with reduced oxygenated compounds and enhanced hydrocarbon content when combined with waste plastics (Amrullah *et al*., 2022; Farobie *et al*., 2024).

To comprehensively analyze the thermal degradation behavior and chemical transformations occurring during pyrolysis, advanced analytical techniques such as thermogravimetric analysis (TGA) and Fourier Transform Infrared Spectroscopy (FTIR) are widely employed. TGA provides critical insights into mass loss and decomposition kinetics, while FTIR identifies chemical functional group evolution during pyrolysis (Liang *et al*., 2019). The combination of TG-FTIR-MS techniques has proven effective in analyzing the co-pyrolysis of various materials, including corn stover and high-density polyethylene (Kai *et al*., 2017), as well as waste tires (Januszewicz *et al*., 2017). These techniques facilitate a detailed understanding of pyrolysis reaction mechanisms, particularly in terms of shifting chemical bonds and decomposition pathways under different thermal conditions (Idris *et al*., 2010; Vuthaluru, 2004). Recent studies have further optimized the bio-oil yield and quality using response surface methodology (RSM), indicating that precise control of temperature and feedstock ratios can significantly enhance fuel properties (Amrullah *et al*., 2024).

Although significant research has been conducted on biomass and waste tire pyrolysis—such as the works of Martínez *et al.* (2014c), Tang *et al.* (2019), and Alvarez *et al.* (2019), which primarily focused on product yields and general compositional trends—studies providing *detailed mechanistic insights* into the thermal degradation behavior and *chemical bond evolution* of biomass–tire mixtures remain scarce. This study specifically addresses this gap by employing combined TGA, FTIR, and GC-MS analyses to elucidate how varying GW-WT ratios influence decomposition pathways and chemical structure transformations, offering a deeper understanding of synergistic interactions in the co-pyrolysis process.

2. Material and Methods

2.1 Sample Preparation

Seaweed waste from Gracilaria (GW) and waste tires (WT) were used as feedstocks for the experimental runs. The Gracilaria waste was obtained from the seaweed home industry, Rumput Laut Mandiri, in Wonosari, Gunung Kidul, Jogjakarta. The seaweed was harvested and processed during the 2023 season, and the residual waste from agar extraction was utilized as feedstock for this study. The waste tires were pre-shredded to a particle size of under 20 mesh. The Gracilaria waste was initially milled and sieved using a 20-mesh screen to obtain fine particles before being dried in an oven at 105°C for 6 hours. The dried samples were then stored in an airtight container to prevent moisture absorption. The GW and WT feedstocks were mixed at mass ratios of 100/0, 75/25, 50/50, 25/75, and 0/100 (w/w) for subsequent experimental procedures.

2.2 Thermogravimetric Analysis (TGA)

Thermal degradation analysis was conducted using a thermogravimetric analyzer (TGA 701, LECO, Model No. 604-100-700) to determine the degradation temperatures, thermal behavior, and theoretical volatility of the samples under an inert nitrogen (N_2) atmosphere. A sample weighing 8.0 mg was placed in an aluminum crucible and heated from room temperature to 700°C at a heating rate of 20°C/min under a constant N_2 flow rate of 20 mL/min. The results from the TGA analysis served as the basis for determining the experimental pyrolysis temperature range.

2.3 Fourier Transform Infrared Spectroscopy (FTIR)

Fourier transform infrared (FTIR) spectroscopy was performed to analyze the spectral characteristics of both the raw materials and the liquid pyrolytic products. The analysis was conducted using an FTIR spectrometer (Bruker-Tensor II) equipped with an attenuated total reflectance (ATR) accessory and a ZnSe/Zinc Selenide beam splitter. FTIR was employed to identify the functional groups present in the feedstocks before pyrolysis and in the liquid products after pyrolysis. Infrared spectra were recorded with a resolution of 4.0 cm^{-1} over a wavenumber range of 4000–500 cm^{-1}.

2.4 Gas Chromatography-Mass Spectrometry (GC-MS)

An analytical technique was conducted using gas chromatography mass spectrometry (GC-MS) to perform detailed chemical characterization of bio-oil components. The chromatographic analysis of the liquid fraction was carried out on an Agilent chromatograph equipped with an Agilent-MS mass spectrometer. The separation was performed on an HP-DMS capillary column (30 mm × 0.25 mm ID × 0.25 μm) at an initial temperature of 50°C, which was maintained for 10 minutes at the final temperature. A 0.5 μL aliquot of the sample was injected for analysis. The identification of compounds was conducted based on a comparison with the NIST library database, using a similarity threshold above 60%. The results were reported in a semi-quantitative manner, based on the relative peak areas in the total ion chromatogram (TIC). No internal standards were used in this analysis. The peak area percentages thus reflect the approximate abundance of each

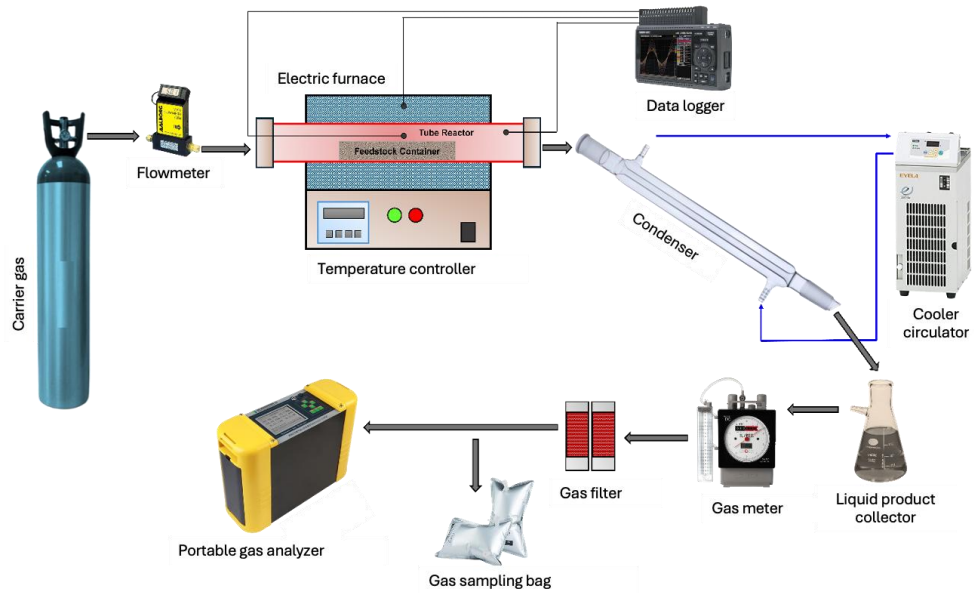

Fig. 1 Schematic diagram of the co-pyrolysis experimental setup

compound relative to the total detected compounds in the sample.

2.5 Pyrolysis Experimental Procedure

The pyrolysis experiments were carried out at atmospheric pressure in a horizontal stainless steel tubular reactor with an inner diameter of 5 cm, an outer diameter of 5.6 cm, and a length of 40 cm. The experimental setup included an N_2 supply, flow meter, tubular pyrolysis reactor, electrically heated furnace with a proportional-integral-derivative (PID) temperature controller, condenser, liquid collection unit, gas meter, gas sampling system, gas filter, and gas analyzer (Figure 1).

3. Results and Discussion

3.1 Thermogravimetric Analysis

The thermogravimetric analysis (TGA) revealed significant thermal decomposition patterns and corresponding reaction rates. Figure 2 presents the TG curves for the five sample mixtures at a heating rate of 20°C/min. The thermogravimetric analysis (TGA) plot elucidates the thermal decomposition behavior of materials with varying compositions, specifically labeled as GW and WT. The TGA results typically reveal weight loss occurring in three distinct stages: the initial release of moisture and volatiles (approximately 0–150°C), followed by primary degradation (150–450°C), and concluding with a stabilization phase (450–700°C). This pattern is consistent with findings in the literature, where TGA has been employed to analyze the thermal stability of various composite materials, indicating that the initial weight loss is often attributed to moisture and volatile components (Xu *et al.*, 2019; Zabihzadeh, 2010). In the context of the GW100+WT0 sample, which demonstrates the highest thermal stability, it is noted that this composition exhibits a slower degradation rate and retains a greater residual weight at elevated temperatures. This observation aligns with studies that have shown how specific material compositions can significantly influence thermal stability and degradation rates. For instance, Zabihzadeh discusses the importance of thermal stability in composite materials, highlighting how variations in composition can lead

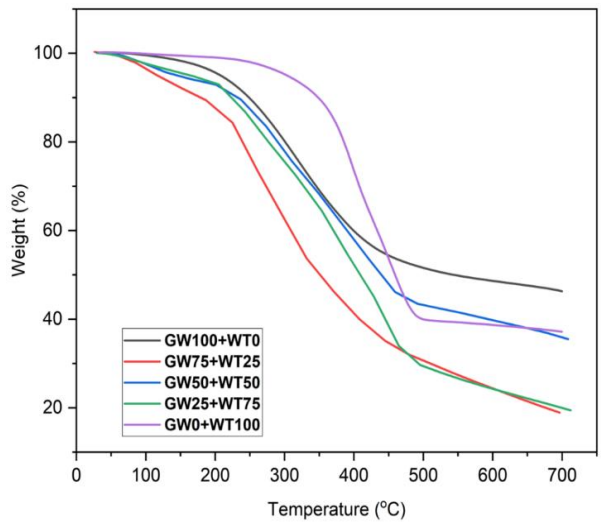

Fig. 2 Thermogravimetry analysis (TGA) curve of Gracilaria (GW), waste tires (WT), and both mixture

to different thermal behaviors (Zabihzadeh, 2010). Similarly, Xu *et al.* (2019) emphasize the role of material composition in determining the thermal degradation characteristics of composites, supporting the assertion that GW enhances thermal stability. Conversely, the GW0+WT100 sample, which is rich in WT, exhibits lower thermal resistance, characterized by an earlier onset of decomposition and reduced char formation. This phenomenon suggests that increased WT content may compromise the structural integrity of the material, leading to more rapid degradation. The literature supports this observation, as studies have indicated that the presence of certain components can adversely affect the thermal stability of composites. For example, Khalil *et al.* (2022) noted that the thermal stability of composites can be influenced by their constituent materials, which can lead to variations in degradation rates and char yield. Furthermore, the kinetic studies on thermal decomposition have shown that the composition of the materials plays a crucial role in determining their thermal behavior, as evidenced by the findings of Islam

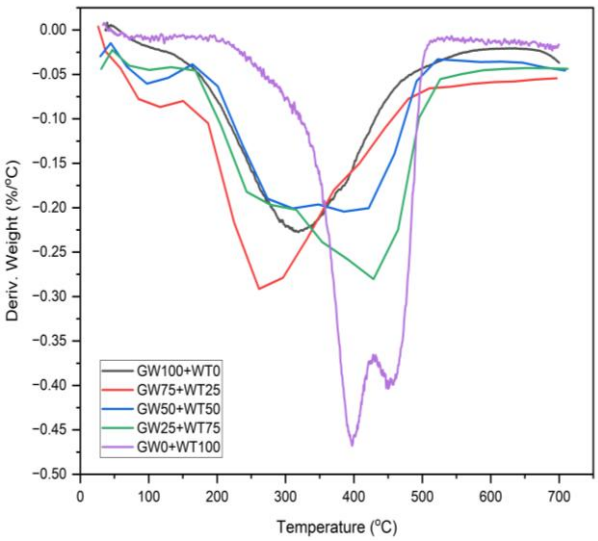

Fig. 3 Derivative Thermogravimetry (DTG) curve of Gracilaria (GW), waste tires (WT), and both mixture

and Gafur (2023), who explored the thermal properties of various composite materials.

Figure 3 shows the Derivative Thermogravimetric (DTG) curve, which represents the rate of weight loss (derivative weight, %/°C) as a function of temperature. The DTG curves obtained from thermogravimetric analysis provide critical insights into the thermal degradation behavior of various samples, particularly in relation to their composition of green waste (GW) and wood waste (WT). The distinct peaks observed in the DTG curves correspond to the maximum degradation rates of the samples, indicating the temperatures at which decomposition occurs most rapidly.

The initial broad peaks in the range of 100–200 °C are primarily attributed to moisture evaporation and the release of low-molecular-weight volatiles. This phenomenon has been documented in studies examining the thermal behavior of natural polymers and composites (Bakirtzis *et al*., 2014). For instance, Bakirtzis *et al.* noted that the addition of fire retardants to lignocellulosic materials resulted in a shift of decomposition profiles towards lower temperatures, which aligns with the observed behavior in the current analysis (Bakirtzis *et al*., 2014). The major decomposition peaks, occurring between 250–500°C, represent the thermal degradation of organic components. Variations in peak temperature and intensity are influenced by the GW and WT composition. Specifically, the GW100+WT0 sample exhibits a relatively higher peak temperature, suggesting enhanced thermal stability, while the GW0+WT100 sample shows a more intense and lower-temperature degradation peak, indicating reduced thermal resistance. This observation is consistent with findings by Yang *et al*., who demonstrated that the thermal stability of materials is significantly influenced by their composition and structure (Yang *et al*., 2017). Furthermore, the results corroborate the work of Çulhaoğlu and Kaya (2015), who highlighted the importance of material composition in determining thermal stability and degradation characteristics. As the WT content increases, the decomposition shifts to lower temperatures, accompanied by sharper peaks that imply a faster degradation rate. This trend suggests that higher WT content compromises thermal stability, a conclusion supported by research indicating that the presence of certain components can accelerate thermal breakdown (Huang *et al*., 2014). For example, Huang *et al.* (2014) discussed how the thermal stability of phase change materials can be affected by their composition, leading to variations in degradation behavior. Additionally, the residual stability observed above 500°C indicates differences in char formation, with GW-rich samples retaining more thermally stable residues. This finding aligns with the work of Rybiński and Janowska, who emphasized the significance of char formation in enhancing thermal stability (Rybiński & Janowska, 2014).

3.2 Fourier Transform Infrared (FTIR)

Thermal The FTIR spectrum of the raw materials is depicted in Figure 4, illustrating the absorption of infrared radiation at various wavelengths. The extent of light absorption at a given wavelength determines the transmittance level, where stronger absorption peaks correspond to lower transmittance values (Z. Wang *et al*., 2023a). The black spectrum represents Gracilaria waste (GW) as the raw material. The peak observed between 3500 and 3700 cm^{-1} is associated with free -OH groups, indicating the presence of alcohol, water, and phenolic compounds (Mecozzi & Sturchio, 2017). The peak at 2981 cm^{-1} corresponds to C-H ring stretching in aromatic groups, while the peaks at 2876 cm^{-1} and 2822 cm^{-1} are linked to C-H bonds in alkanes and aldehydes, respectively. The presence of alkanes is further verified by the C-H vibrations occurring within the 3000–2800 cm^{-1} range. Additionally, the peaks at 2357 and 2332 cm^{-1} correspond to C=O and N=C=O bonds in hemicellulose, confirming the presence of aldehydes, ketones, and carbonyl groups. The peak at 2294 cm^{-1} represents C≡N stretching of nitriles, while the band between 2260 and 2210 cm^{-1} further verifies the presence of nitrile groups. The peaks at 1055 and 1033 cm^{-1} indicate C-O stretching in alcohol compounds, whereas those at 1008 and 875 cm^{-1} correspond to C=C bonds in benzene and alkenes. The identification of OH as H_2O and CO suggests the release of oxygen during the pyrolysis process. The formation of H_2O primarily results from hydroxyl dehydration reactions associated with cellulose and hemicellulose in the algal biomass. Meanwhile, the production of alcohols, aldehydes, and ketones is mainly driven by the pyrolytic breakdown of cellulose and hemicellulose.

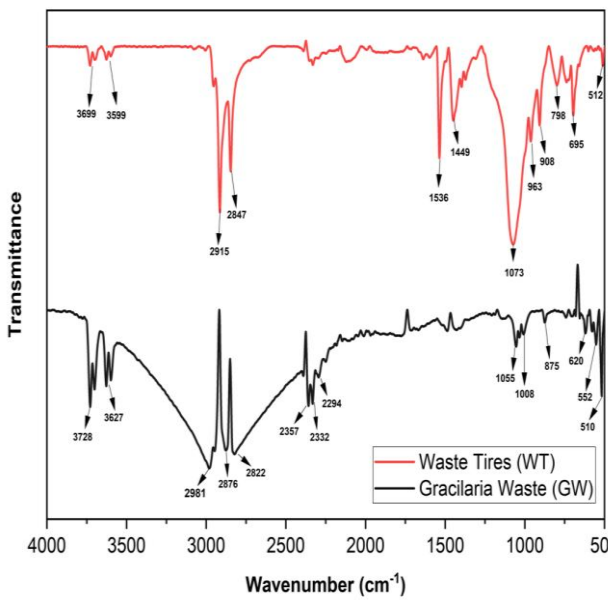

Fig. 4 FTIR Spectrum of raw materials of GW and WT

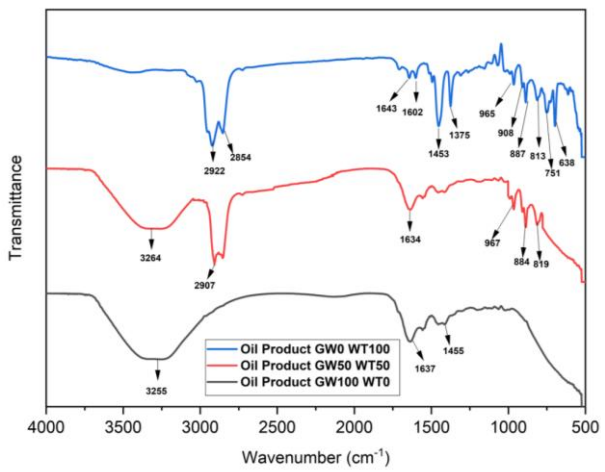

Fig. 5 FTIR spectrum of liquid products

Figure 5 show the FTIR spectra of the chemical composition of oil products derived from varying ratios of Gracilaria waste (GW) and waste tires (WT). The black spectrum (GW100+WT0), which represents 100% Gracilaria waste, reveals a broad O-H stretching peak at 3265 cm^{-1}. This peak indicates the presence of hydroxyl groups, likely from alcohols or water, and is consistent with findings from previous studies that have identified similar functional groups in biomass-derived oils (Forero-Doria *et al.*, 2015). The strong C=O stretching observed at 1637 cm^{-1} suggests the presence of aldehydes, ketones, or carboxyl compounds resulting from biomass decomposition, which aligns with the thermal degradation characteristics reported in the literature (Puri *et al.*, 2024). In contrast, the blue spectrum (GW0+WT100), derived solely from waste tires, exhibits peaks at 2924 cm^{-1} and 2852 cm^{-1}, corresponding to C-H stretching vibrations typical of alkanes. The multiple peaks in the fingerprint region (1025, 975, 913, 833, and 754 cm^{-1}) signify the presence of aromatic and aliphatic hydrocarbons, which are characteristic of tire pyrolysis products (Bakirtzis *et al.*, 2014). This observation is supported by the work of Onay, who discussed the chemical composition of pyrolysis products from waste tires, highlighting the prevalence of hydrocarbon structures (Onay, 2014). The red spectrum (GW50+WT50), obtained from an equal mixture of GW and WT, illustrates a blend of both biomass and tire-derived compounds, indicating the complexity of the chemical interactions during co-pyrolysis. These spectral characteristics correspond to functional bonds and wavenumber ranges identified in FTIR spectroscopy, as detailed in the Table 1.

To provide a more quantitative perspective on the FTIR results, we analyzed the relative intensity changes of key characteristic bands across different GW-WT mixtures. The intensities of the hydroxyl (-OH) stretching band (~3265 cm^{-1}), carbonyl (C=O) stretching band (~1637 cm^{-1}), and aromatic C=C stretching band (1620–1420 cm^{-1}) were normalized against the C-H alkanes stretching band (3000–2850 cm^{-1}) as an internal reference. The normalized intensity of the -OH band was observed to decrease progressively with increasing WT content, consistent with reduced oxygenated compound formation. Similarly, the C=O band intensity showed a marked reduction from pure GW100 to GW50+WT50 and further to pure WT, confirming the suppression of carbonyl-containing compounds. Conversely, the aromatic C=C band intensity increased with higher WT ratios, reflecting the enrichment of hydrocarbon structures in the pyrolysis products. These semi-quantitative trends corroborate the chemical shifts observed in the GC-MS analysis and demonstrate the synergistic chemical bond evolution during co-pyrolysis.

The -OH free stretching bond at 3800–3500 cm^{-1} indicates free alcohols, while C-H stretching in alkanes (3000–2850 cm^{-1}) confirms the presence of hydrocarbon chains. Aldehyde stretching (2830–2695 cm^{-1}) and CO_2 stretching (~2350 cm^{-1}) further support the oxygenated nature of biomass-derived oils, while C≡C bonds in alkynes (2260–2100 cm^{-1}) and C=C stretching in aromatic rings (1620–1420 cm^{-1}) indicate unsaturated hydrocarbons. Additionally, C-N and C-O stretching (1250–1020 cm^{-1}) suggest aliphatic amines and oxygenated organic groups, whereas bending vibrations of alkenes and aromatics (1000–650 cm^{-1}) confirm structural characteristics of these compounds. The trans C-H bending (990–940 cm^{-1}), benzene ring C-H bending (900–675 cm^{-1}), and out-of-plane C-H bending in benzene (810–750 cm^{-1}) help determine aromatic substitution patterns, while sp^2 hybridized C-H bending (616–519 cm^{-1}) is indicative of benzene and aromatic systems. This table serves as a crucial reference for interpreting FTIR spectra and characterizing hydrocarbons, oxygenated compounds, and aromatic structures present in the pyrolysis products of Gracilaria waste and waste tires.

3.3 Gas Chromatography-Mass Spectrometry (GC-MS)

A detailed chemical component analysis of the bio-oil was carried out using GC–MS. The compounds in the liquid product (bio-oil) were identified by comparing the chromatogram

Table 1
Functional chemical bond and wavelength range

No.	Functional bonds	Wavelength (cm^{-1})	Group
1	-OH free	3800-3500	stretching, free alcohol
2	C-H alkanes	3000-2850	stretching alkanes
3	H-C=O, C-H	2830-2695	stretching aldehydes
4	O=C=O	~2350	stretching CO_2
5	-C=C- alkynes	2260-2100	stretching alkynes
6	C=C	1620-1420	Aromatic heteroatomic rings
7	C-N, C-O	1250-1020	stretching aliphatic amines and C-O stretching
8	=C-H	1000-650	bending alkenes
9	-C-H	990-940	bending trans RCH=CHR
10	C-H benzene	900-675	C-H aromatics benzene
11	-C-H	810-750	-C-H out of plane bending, m-subst., benzene
12	-C-H	790-650	-C-H bending cis RCH=CHR
13	C-H	616, 519	C-H bending, alkene sp2 C-H aromatic sp2

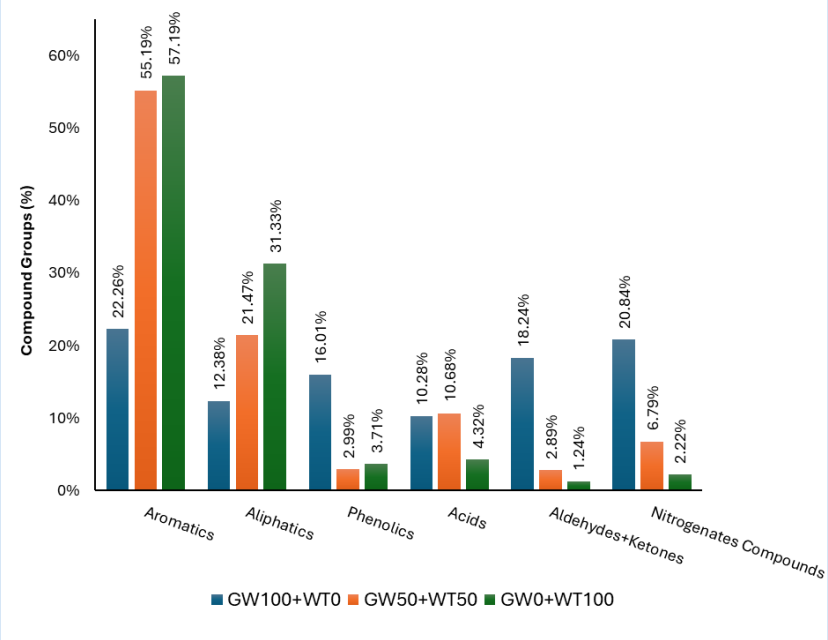

Fig. 6 The compound groups of bio-oil products

obtained from the standards. The pyrolysis bio-oil was a complicated mixture containing a wide range of chemical compounds.

Figure 6 shows GC–MS analysis of bio-oils with different mixture ratios of GW and WT content. Only the compounds with a relative similarity with the database higher than 60% are listed. It is observed that the liquid product contains many compound groups with different concentrations. Those compounds can be grouped as aromatics, aliphatics, phenolics, acids, aldehydes ketones, and nitrogenates compounds. Based on the three samples, bio-oil from GW100+WT0 contains more aromatics, aldehydes ketones, and nitrogenates compound groups. While bio-oil from GW50+WT50 and GW0+WT100 contains more aromatics and aliphatic compounds. Figure 6 also shows that the higher the WT ratio in raw materials, the higher the content of aromatic compounds in bio-oil products. Likewise, the aliphatic content in bio-oil will increase along with the increasing WT ratio in feedstock. This may be due to thermal instability and the breakdown of polymers and other long-chain compounds into smaller fragments during pyrolysis. The major chemical constituents of Gracilaria waste (GW) are carbohydrates, while waste tires (WT) contains many polymer compounds derived from petroleum. Accordingly, the major pyrolysis products and condensed bio-oil are derived from these components with different proportions depending on the feedstock mixture.

It is clear that the concentration of phenolics, aldehydes and ketones, and nitrogenates compounds in the bio-oil of both GW50+WT50 and GW0+WT100 was less than that for the bio-oil of pure Gracilaria (GW100+WT0). This can be attributed to the removal of oxygenated compounds during the addition of waste tire into Gracilaria. Adding WT to GW pyrolysis leads to a bio-oil with a different chemical composition. These compositional shifts can be explained by the underlying chemical mechanisms occurring during co-pyrolysis. The thermal cracking of waste tire polymers leads to random scission of C-C and C-H bonds, generating a high concentration of alkyl and hydrogen radicals (R• and H•). The presence of these radicals facilitates hydrogen transfer reactions that stabilize oxygenated intermediates derived from the biomass, leading to a reduction in aldehydes, ketones, and phenolic compounds. Moreover, the H• radicals promote hydrodeoxygenation, converting oxygenated groups into water and hydrocarbons. In parallel, the scission of polymer chains from WT contributes to an increased formation of aromatic and aliphatic hydrocarbons, as detected in the GC-MS results. The synergistic effect between biomass and WT radicals thereby shifts the bio-oil composition toward higher hydrocarbon content while suppressing oxygenates and nitrogenates, consistent with the trends observed in our study. Similar radical-mediated mechanisms have been reported in co-pyrolysis systems by Tang *et al.* (2019) and Martínez *et al.* (2014c). It was evident that the hydrocarbon content was significantly increased with the addition of WT, and the relative contents of hydrocarbons increased as the WT share increased in the blends. Whereas an increase in WT content resulted in a decrease in nitrogenated and oxygenated compounds compared to pure GW biomass. When the WT percentage was 50%, the nitrogenate compounds were expectedly decreases from 20.84% to 6.79 %, and with pure WT (GW0+WT100) contains only 2.22% of nitrogenated compounds. Additionally, the aldehydes and ketones decrease significantly with the addition of WT50%, followed by pure WT100%. The decrease occurred from 18.24% in GW100+WT0 to 2.89% and 1.24% in GW50+WT50 and GW0+WT100, respectively. This phenomenon is primarily due to the free radicals preventing amino acids from reacting with long-chain aliphatic acids to form amides (Kumar *et al.*, 2022). This observation may be attributed to the interaction of H radicals derived from WT with the C=O double bonds of aldehydes or the C-CO bonds in ketones, consequently leading to CO generation (Tang *et al.*, 2019).

A comparable advantageous impact of WT has been reported in prior research concerning various types of biomass. Alvarez *et al.* (2019) examined the co-pyrolysis process involving lignocellulosic biomass and waste tires, noting that adding waste tires significantly reduced the presence of oxygenated compounds while concurrently enhancing the synthesis of hydrocarbons. Sanahuja Parejo *et al.* (2018) reported an increase in the production of cyclic hydrocarbons

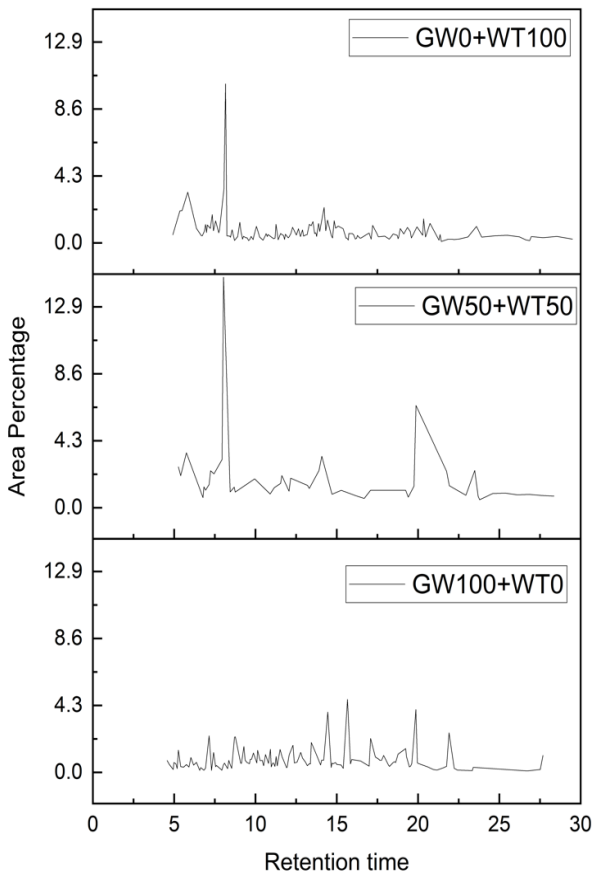

Fig. 7 The chromatograms of three bio-oil samples with various feedstocks

and reduce the phenolic compounds when waste tires were co-pyrolyzed with grape seeds. The presence of high carbon and hydrogen material promoted the decomposition of oxygenated compounds from biomass, inhibiting the generation of aldehyde, ketone, and furan groups (Yuan *et al*., 2018). Similarly, Martinez *et al.* observed that adding waste tires to the biomass pyrolysis decreased the amount of ketones, aldehydes, and phenolic compounds in the bio-oil (Martínez *et al*., 2014a).

Figure 7 shows the chromatograms of three bio-oil samples by GC-MS method in spectrum mode. As seen in chromatograms, the samples showed different peak intensities in qualitative profiles. The results of peak identification are shown in Table A1, A2, and A3 for the three samples. These tables contain the compounds, retention times, and area percentages. The bio-oil derived from GW pyrolysis (GW100+WT0) exhibited relatively high nitrogenate compounds of 20.84% and oxygenated content of 34.25%. On the other hand, the bio-oil from WT pyrolysis (GW0+WT100) was characterized by a markedly lower presence of nitrogenate and oxygenate compounds (7.17%), with a significant content of hydrocarbon compounds (88.52%). We can conclude that adding WT to the GW prior to biomass pyrolysis increases the concentrations of hydrocarbon compounds (aromatics and aliphatic groups) in the bio-oil product.

4. Conclusion

This study highlights the potential of co-pyrolyzing Gracilaria waste (GW) and waste tires (WT) to enhance bio-oil properties, particularly by improving hydrocarbon content and reducing oxygenated compounds. The thermogravimetric analysis (TGA) results demonstrated that the thermal degradation of the mixture shifted towards higher temperatures, indicating improved thermal stability. The Fourier Transform Infrared Spectroscopy (FTIR) analysis revealed significant transformations in chemical bonds, with a decrease in hydroxyl (-OH) groups and an increase in hydrocarbon-related bonds (C-H, C=C, and C-C), which contribute to the improved fuel quality of the liquid product. These findings contribute to the broader field of biomass conversion and waste valorization by demonstrating the synergistic effects of co-pyrolysis between marine biomass and polymeric waste. The study provides valuable insights into the chemical interactions that occur during co-pyrolysis, offering a feasible approach to optimizing bio-oil composition for potential applications in renewable energy and sustainable waste management. Further research should explore the influence of reaction conditions, such as catalyst addition and temperature variations, on product composition and yield. Additionally, the long-term stability and upgradability of the derived bio-oil should be assessed to facilitate its practical implementation in energy applications.

Acknowledgments

I would like to express my gratitude to the National Research and Innovation Agency for the financial support in conducting this study.

Author Contributions: I.M.: Conceptualization, preparation of equipment and materials, collection of experimental data, data analysis, writing the original draft of manuscript, S.E.M.; supervision, resources, and review, D.A.S.; monitoring, review and editing, project supervision, and validation, A.A.; manuscript review, editing, and validation, W.J.Y.; supervision, manuscript review, and validation. All authors have read and agreed to the published version of the manuscript.

Funding: This research was funded by the Degree by Research Program of the National Research and Innovation Agency year 2024.

Conflicts of Interest: The authors declare no conflict of interest.

References

Abnisa, F., & Wan Daud, W. M. A. (2014). A review on co-pyrolysis of biomass: An optional technique to obtain a high-grade pyrolysis oil. *Energy Conversion and Management*, *87*, 71–85. https://doi.org/10.1016/j.enconman.2014.07.007

Alvarez, J., Amutio, M., Lopez, G., Santamaria, L., Bilbao, J., & Olazar, M. (2019). Improving bio-oil properties through the fast co-pyrolysis of lignocellulosic biomass and waste tyres. *Waste Management*, *85*, 385–395. https://doi.org/10.1016/j.wasman.2019.01.003

Alzahrani, N., Nahil, M. A., & Williams, P. T. (2025). Co-pyrolysis of waste plastics and tires: Influence of interaction on product oil and gas composition. *Journal of the Energy Institute*, *118*(October 2024), 101908. https://doi.org/10.1016/j.joei.2024.101908

Amrullah, A., Farobie, O., and Ernawati, L. (2023). *Slow-pyrolysis of brown macroalgae Padina sp.: Product characterization and degradation kinetic mechanism*. 1–19. http://dx.doi.org/10.21203/rs.3.rs-2548474/v1

Amrullah, A., Farobie, O., Irawansyah, H., Lutfi, M., & Noviani Haty, L. (2024). Synergistic enhancement of bio-oil production, quality, and optimization from co-pyrolysis purun tikus (Eleocharis dulcis) and plastic waste using response surface methodology.

Process Safety and Environmental Protection, *187*(January), 471–482. https://doi.org/10.1016/j.psep.2024.04.079

Amrullah, A., Farobie, O., Septarini, S., & Satrio, J. A. (2022). Synergetic biofuel production from co-pyrolysis of food and plastic waste: reaction kinetics and product behavior. *Heliyon*, *8*(8). https://doi.org/10.1016/j.heliyon.2022.e10278

Bakirtzis, D., Tsapara, V., Kolovos, K. G., & Liodakis, S. (2014). Assessment of the Impact of Fire Retardants on the Combustion of Natural Polymers Employing DTG and LOI. *Fire and Materials*, *39*(2), 109–118. https://doi.org/10.1002/fam.2232

Chen, W. H., Naveen C, Ghodke, P. K., Sharma, A. K., & Bobde, P. (2023). Co-pyrolysis of lignocellulosic biomass with other carbonaceous materials: A review on advance technologies, synergistic effect, and future prospectus. *Fuel*, *345*(December 2022), 128177. https://doi.org/10.1016/j.fuel.2023.128177

Çulhaoğlu, S., & Kaya, İ. (2015). Synthesis, Characterization, Thermal Stability and Conductivity of New Schiff Base Polymer Containing Sulfur and Oxygen Bridges. *Polymer Korea*, *39*(2), 225–234. https://doi.org/10.7317/pk.2015.39.2.225

Farobie, O., Amrullah, A., Fatriasari, W., Nandiyanto, A. B. D., Ernawati, L., Karnjanakom, S., Lee, S. H., Selvasembian, R., Azelee, N. I. W., & Aziz, M. (2024). Co-pyrolysis of plastic waste and macroalgae Ulva lactuca, a sustainable valorization approach towards the production of bio-oil and biochar. *Results in Engineering*, *24*(October), 103098. https://doi.org/10.1016/j.rineng.2024.103098

Forero-Doria, O., Gallego, J., Valdés, O., Pinzon-Topal, C., Santos, L. S., & Guzmán, L. (2015). Relationship Between Oxidative Stability and Antioxidant Activity of Oil Extracted From the Peel of Mauritia Flexuosa Fruits. *Journal of Thermal Analysis and Calorimetry*, *123*(3), 2173–2178. https://doi.org/10.1007/s10973-015-4822-7

González, A., Penedo, M., Mauris, E., Fernández-Berridi, M. J., Irusta, L., & Iruin, J. (2010). Pyrolysis analysis of different Cuban natural fibres by TGA and GC/FTIR. *Biomass and Bioenergy*, *34*(11), 1573–1577. https://doi.org/10.1016/j.biombioe.2010.06.004

Huang, X., Xia, W., & Zou, R. (2014). Nanoconfinement of Phase Change Materials Within Carbon Aerogels: Phase Transition Behaviours and Photo-to-Thermal Energy Storage. *Journal of Materials Chemistry A*, *2*(47), 19963–19968. https://doi.org/10.1039/c4ta04605f

Hussain, Z., Khan, A., Naz, M. Y., Jan, M. R., Khan, K. M., Perveen, S., Ullah, S., & Shukrullah, S. (2021). Borax-catalyzed valorization of waste rubber and polyethylene using pyrolysis and copyrolysis reactions. *Asia-Pacific Journal of Chemical Engineering*, *16*(5), 1–12. https://doi.org/10.1002/apj.2696

Idris, S. S., Rahman, N. A., Ismail, K., Alias, A. B., Rashid, Z. A., & Aris, M. J. (2010). Investigation on thermochemical behaviour of low rank Malaysian coal, oil palm biomass and their blends during pyrolysis via thermogravimetric analysis (TGA). *Bioresource Technology*, *101*(12), 4584–4592. https://doi.org/10.1016/j.biortech.2010.01.059

Islam, N., & Gafur, M. A. (2023). Matrix-Material Fabrication Technique and Thermogravimetric Analysis of Banana Fiber Reinforced Polypropylene Composites. *Journal of Building Material Science*, *5*(2), 15–24. https://doi.org/10.30564/jbms.v5i2.5700

Januszewicz, K., Klein, M., Klugmann-Radziemska, E., & Kardas, D. (2017). Thermogravimetric analysis/pyrolysis of used tyres and waste rubber. *Physicochemical Problems of Mineral Processing*, *53*(2), 802–811. https://doi.org/10.5277/ppmp170211

Kai, X., Li, R., Yang, T., Shen, S., Ji, Q., & Zhang, T. (2017). Study on the co-pyrolysis of rice straw and high density polyethylene blends using TG-FTIR-MS. *Energy Conversion and Management*, *146*, 20–33. https://doi.org/10.1016/j.enconman.2017.05.026

Khalil, Y., Hopkinson, N., Kowalski, A., & Fairclough, J. P. A. (2022). Investigating the Feasibility of Processing Activated Carbon/Uhmwpe Polymer Composite Using Laser Powder Bed Fusion. *Polymers*, *14*(16), 3320. https://doi.org/10.3390/polym14163320

Kim, J. S. (2015). Production, separation and applications of phenolic-rich bio-oil - A review. *Bioresource Technology*, *178*, 90–98. https://doi.org/10.1016/j.biortech.2014.08.121

Kumar, A., Yan, B., Tao, J., Li, J., Kumari, L., Tafa Oba, B., Akintayo Aborisade, M., Ali Jamro, I., & Chen, G. (2022). Co-pyrolysis of de-oiled microalgal biomass residue and waste tires: Deeper insights from thermal kinetics, behaviors, drivers, bio-oils, bio-chars, and in-situ evolved gases analyses. *Chemical Engineering Journal*, *446*(P2), 137160. https://doi.org/10.1016/j.cej.2022.137160

Li, C., Liu, Z., Yu, J., Hu, E., Zeng, Y., & Tian, Y. (2023). Cross-interaction of volatiles in fast co-pyrolysis of waste tyre and corn stover via TG-FTIR and rapid infrared heating techniques. *Waste Management*, *171*(July), 421–432. https://doi.org/10.1016/j.wasman.2023.09.037

Liang, B., Wang, J., Hu, J., Li, C., Li, R., Liu, Y., Zeng, K., & Yang, G. (2019). TG-MS-FTIR study on pyrolysis behavior of phthalonitrile resin. *Polymer Degradation and Stability*, *169*, 108954. https://doi.org/10.1016/j.polymdegradstab.2019.108954

Ma, Y., Qi, H., Zhang, J., Cui, P., Zhu, Z., & Wang, Y. (2023). Thermodynamic analysis of a carbon capture hydrogen production process for end-of-life tires using plasma gasification. *Journal of Cleaner Production*, *384*(October 2022), 135662. https://doi.org/10.1016/j.jclepro.2022.135662

Martínez, J. D., Veses, A., Mastral, A. M., Murillo, R., Navarro, M. V., Puy, N., Artigues, A., Bartrolí, J., & García, T. (2014a). Co-pyrolysis of biomass with waste tyres: Upgrading of liquid bio-fuel. *Fuel Processing Technology*, *119*, 263–271. https://doi.org/10.1016/j.fuproc.2013.11.015

Masfuri, I., Amrullah, A., Farobie, O., Anggoro, T., Rian S, F., Prabowo, W., & Rosyadi, E. (2024). Temperature effects on chemical reactions and product yields in the Co-pyrolysis of wood sawdust and waste tires: An experimental investigation. *Results in Engineering*, *23*(July), 102638. https://doi.org/10.1016/j.rineng.2024.102638

Mavukwana, A. E., Stacey, N., Fox, J. A., & Sempuga, B. C. (2021). Thermodynamic comparison of pyrolysis and gasification of waste tyres. *Journal of Environmental Chemical Engineering*, *9*(2), 105163. https://doi.org/10.1016/j.jece.2021.105163

Mecozzi, M., & Sturchio, E. (2017). Computer assisted examination of infrared and near infrared spectra to assess structural and molecular changes in biological samples exposed to pollutants: A case of study. *Journal of Imaging*, *3*(1). https://doi.org/10.3390/jimaging3010011

Onay, Ö. (2014). The catalytic Co-pyrolysis of waste tires and pistachio seeds. *Energy Sources, Part A: Recovery, Utilization and Environmental Effects*, *36*(18), 2070–2077. https://doi.org/10.1080/15567036.2013.791900

Puri, L., Hu, Y., & Naterer, G. F. (2024). Critical Review of the Role of Ash Content and Composition in Biomass Pyrolysis. *Front. Fuels*, *2*. https://doi.org/10.3389/ffuel.2024.1378361

Prasetiawan, H., Selvia Fardhyanti, D., Hadiyanto, H., . Fatriasari, W. (2024). Catalytic Pyrolysis of Biomass Waste Mixture over Activated Carbon and Zeolite Catalyst for the Production Bio Oil. *Key Engineering Materials*, 978, 107–117. Trans Tech Publications, Ltd. https://doi.org/10.4028/p-9igsfm

Rybiński, P., & Janowska, G. (2014). Effect of the Spatial Network Structure and Cross-Link Density of Diene Rubbers on Their Thermal Stability and Fire Hazard. *Journal of Thermal Analysis and Calorimetry*, *117*(1), 377–386. https://doi.org/10.1007/s10973-014-3673-y

Sanahuja-Parejo, O., Veses, A., Navarro, M. V., López, J. M., Murillo, R., Callén, M. S., & García, T. (2018). Catalytic co-pyrolysis of grape seeds and waste tyres for the production of drop-in biofuels. *Energy Conversion and Management*, *171*(May), 1202–1212. https://doi.org/10.1016/j.enconman.2018.06.053

Tang, Z., Chen, W., Chen, Y., Yang, H., & Chen, H. (2019). Co-pyrolysis of microalgae and plastic: Characteristics and interaction effects. *Bioresource Technology*, *274*, 145–152. https://doi.org/10.1016/j.biortech.2018.11.083

Vuthaluru, H. B. (2004). Thermal behaviour of coal/biomass blends during co-pyrolysis. *Fuel Processing Technology*, *85*(2–3), 141–155. https://doi.org/10.1016/S0378-3820(03)00112-7

Wang, F., Gao, N., Magdziarz, A., & Quan, C. (2022). Bioresource Technology Co-pyrolysis of biomass and waste tires under high-pressure two-stage fixed bed reactor. *Bioresource Technology*, *344*(PB), 126306. https://doi.org/10.1016/j.biortech.2021.126306

Wang, Z., Wu, M., Chen, G., Zhang, M., Sun, T., Burra, K. G., Guo, S., Chen, Y., Yang, S., Li, Z., Lei, T., & Gupta, A. K. (2023a). Co-pyrolysis characteristics of waste tire and maize stalk using TGA, FTIR and Py-GC/MS analysis. *Fuel*, *337*(October 2022). https://doi.org/10.1016/j.fuel.2022.127206

Xu, S., Uzoejinwa, B. B., Wang, S., Hu, Y., Qian, L., Liu, L., Li, B., He, Z., Wang, Q., Abomohra, A. E. F., Li, C., & Zhang, B. (2019). Study on co-pyrolysis synergistic mechanism of seaweed and rice husk by investigation of the characteristics of char/coke. *Renewable Energy*, *132*, 527–542. https://doi.org/10.1016/j.renene.2018.08.025

Yang, P., Han, S., Su, J., Wang, Y., Zhang, X., Han, N., & Li, W. (2017). Design of Self-healing Microcapsules Containing Bituminous Rejuvenator With Nano-CaCO₃/Organic Composite Shell: Mechanical Properties, Thermal Stability, and Compactability. *Polymer Composites*, *39*(S3). https://doi.org/10.1002/pc.24343

Yuan, H., Fan, H., Shan, R., He, M., Gu, J., & Chen, Y. (2018). Study of synergistic effects during co-pyrolysis of cellulose and high-density polyethylene at various ratios. *Energy Conversion and Management*, *157*(October 2017), 517–526. https://doi.org/10.1016/j.enconman.2017.12.038

Zabihzadeh, S. M. (2010). Influence of Plastic Type and Compatibilizer on Thermal Properties of Wheat Straw Flour/Thermoplastic Composites. *Journal of Thermoplastic Composite Materials*, *23*(6), 817–826. https://doi.org/10.1177/0892705709353711

Zhang, M., Qi, Y., Zhang, W., Wang, M., Li, J., & Lu, Y. (2024). *A review on waste tires pyrolysis for energy and material recovery from the optimization perspective*. *199*(February). https://doi.org/10.1016/j.rser.2024.114531

Appendix

Table A1.
The GC-MS analysis of bio-oil GW100+WT0 pyrolysis

Compounds	R.T.	%	Compounds	R.T.	%
Aromatics and Benzene derivatives			**Acids**		
Pyridine, 2-methyl-	4.57	0.77	Creatinine	13.44	1.92
4-Aminopyridine	4.70	0.50	2,3-Dimethylphenyl isocyanate	14.76	0.55
2-Furanmethanol	5.11	0.55	Hexadecanoic acid, methyl ester	19.46	0.35
Pyridine, 3-methyl-	5.26	1.42	n-Hexadecanoic acid	19.87	4.03
Benzene, 1,3-dimethyl-	5.40	0.37	Cyclopropanecarboxylic acid	20.60	0.35
2,6-Lutidine	5.57	0.33	Methyl-10-pentadecenoate	21.16	0.15
Pyridine, 2-ethyl-	5.91	0.35			
1H-Pyrrole, 2,5-dimethyl-	6.19	0.47	**Aldehydes & Ketones**		
Pyridine, 2,5-dimethyl-	6.37	0.64	Ethanone, 1-(2-furanyl)-	6.03	0.96
Pyridine, 2,3-dimethyl-	6.57	0.13	2-Cyclopenten-1-one, 2,3-dimethyl-	8.09	0.60
Pyridine, 3-ethyl-	6.83	0.14	Ethanone, 1-(1H-pyrrol-2-yl)	8.54	0.27
2,4-Dimethylfuran	6.94	0.29	2(1H)-Pyridone, 6-methyl-	9.48	0.64
1H-Pyrrole, 2-ethyl-4-methyl-	7.55	0.36	2-Piperidinone	10.41	0.77
Pyridine, 5-ethyl-2-methyl-	7.93	0.14	2,4-Imidazolidinedione	12.30	1.74
Limonene	8.02	0.46	5-Isopropyl-2,4-imidazolidinedione	15.66	4.68
Indene	8.28	0.24	3-Methyl-1,4-dione	17.37	0.98
3-Pyridinol, TMS derivative	9.63	0.56	2-Hexadecanone	18.18	0.47
Benzofuran, 4,7-dimethyl-	10.97	0.36	2-Pentadecanone, 6,10,14-trimethyl-	18.62	0.64
Indole	12.08	1.13	18-Nor-estra-1,3,5,9-tetraen-12-one	19.55	0.41
1H-Indole, 7-methyl-	13.38	0.54	2,5-Piperazinedione, 3-benzyl-6-isopropyl-	22.42	0.15
1H-Indole, 2,6-dimethyl-	14.66	0.32			
1,2,3,4-Tetrahydro-.beta.-carboline	15.40	0.26	**Nitrogenates Compounds**		
3-Benzyl-4-hydroxy-4H-1,2,4-triazole	15.92	0.83	Isoamyl cyanide	4.98	0.64
2H-Tetrazol, 2-(phenylmethyl)-	18.24	0.38	Tricyclo-hex-3-ene-3-carbonitrile	7.30	0.13
Octahydrodipyrrolo-pyrazine	19.75	2.31	Benzyl nitrile	9.76	0.84
Pyrrolo[1,2-a]pyrazine-1,4-dione, hexahydro-3-(phenylmethyl)-	23.40	0.33	2,3-Pyridinediamine	10.09	0.61
Boscartol F	26.72	0.10	Benzenepropanenitrile	11.27	1.02
			2-Propenenitrile, 3-phenyl-	11.33	0.42
Aliphatics			Diethylpropion	14.45	3.87
1,3,5,7-Cyclooctatetraene	5.75	0.50	Phenylpropanamide	15.00	0.51
Dodecane	10.62	1.14	Cyclo(L-prolyl-L-valine)	18.77	1.17
Cyclodecane, methyl-	11.95	0.34	Hexadecanenitrile	19.24	1.53
Dodecane, 2,6,11-trimethyl-	13.09	0.64	Tetradecanamide	19.95	0.62
Cyclopropane, nonyl-	13.33	0.57	1-ethane-1,1,2,2-tetracarbonitrile	20.00	0.58
4-Oxatricyclo[4.3.1.1(3,8)]undecane	14.07	0.79	Tetradecanamide	20.94	0.18
Pentadecane	14.71	0.60	Hexadecanamide	21.91	2.55
Heptadecane	17.08	2.18	N-Methyldodecanamide	22.22	0.26
1,2-Dioctylcyclopropene	19.29	1.01			
Cholesta-3,5-diene	27.68	1.09			
Phenolics					
Phenol	7.15	2.34			
Phenol, 2-methyl-	8.36	0.77			
p-Cresol	8.71	2.26			
p-Cresol 2	8.76	2.28			
Phenol, 2,4-dimethyl-	9.87	1.25			
Phenol, 4-ethyl-	10.14	1.41			
Phenol, 3-ethyl-5-methyl-	11.04	0.58			
Phenol, 2-ethyl-5-methyl-	11.20	0.38			
Cholesta-4,6-dien-3-ol	27.52	0.19			

Table A2.
The GC-MS analysis of bio-oil GW50+WT50 pyrolysis

Compounds	R.T.	%	Compounds	R.T.	%
Aromatics and Benzene derivatives			Tricosane	22.94	0.80
Ethylbenzene	5.26	2.62	Tetracosane	23.79	0.51
Benzene, 1,3-dimethyl-	5.40	2.06	Pentacosane	24.59	0.91
Benzene, propyl-	6.77	0.65	Hexacosane	25.36	0.94
Benzene, 1-ethyl-4-methyl-	6.94	1.12	Heneicosane	26.10	0.83
Alpha.-Methylstyrene	7.24	2.37	Nonacosane	26.84	0.86
p-Cymene	7.94	3.09	Heptacosane, 1-chloro-	27.55	0.79
D-Limonene	8.03	14.79			
p-Cresol	8.70	1.32	**Phenolics**		
1H-Indene, 1-methyl-	9.95	1.85	Phenol	7.15	1.49
Benzothiazole	11.16	1.28	Phenol, 3-methyl-	8.75	1.00
1H-Indene, 1,3-dimethyl-	11.55	1.56			
1H-Indene, 1,1-dimethyl-	11.62	2.06	**Acids**		
Benzene, 1-cyclopenten-1-yl-	12.17	1.90	n-Hexadecanoic acid	19.88	6.56
Biphenyl	13.31	1.24	Octadecanoic acid	21.76	2.34
Naphthalene, 2,7-dimethyl-	13.90	2.38			
Quinoline, 1,2-dihydro-2,2,4-trimethyl-	14.08	3.30	**Aldehydes & Ketones**		
Naphthalene, 1,6,7-trimethyl-	15.28	1.12	Benzenepropanal	8.45	1.02
Benzene, 1,1'-(1,3-propanediyl)bis-	16.69	0.60	Octahydrodipyrrolo, 10-dione	19.75	1.39
Gamma.-Elemene	19.40	0.68			
			Nitrogenates Compounds		
Aliphatics			2-(Methylthio)phenyl isothiocyanate	16.17	0.77
1,3,5,7-Cyclooctatetraene	5.75	3.52	Hexadecanenitrile	19.24	1.11
1,5-Cyclooctadiene, 1,5-dimethyl-	6.83	1.34	Hexadecanamide	21.92	1.42
cis-2,6-Dimethyl-2,6-octadiene	7.45	2.17	1,4-Benzenediamine, N-(1,3-dimethylbutyl)	23.48	2.40
Tridecane	12.06	1.06	Octadecanamide	23.70	0.73
1,2,3-Trimethylindene	13.20	1.43			
Pentadecane	14.71	0.86			
Heptadecane	17.08	1.13			

Table A3.
The GC-MS analysis of bio-oil GW0+WT100 pyrolysis

Compounds	R.T.	%	Compounds	R.T.	%
Aromatics and Benzene derivatives			Cyclohexene, 1-methyl-4-(1-methylethenyl)	7.79	0.86
Ethylbenzene	5.35	2.06	p-Mentha-1,5,8-triene	8.56	0.85
p-Xylene	5.49	2.08	Cyclohexene, 1-methyl-4-(1-methylethylidene)-	9.04	1.32
Styrene	5.84	3.25	Undecane	9.20	0.25
Benzene, (1-methylethyl)-	6.37	0.94	Cyclohexene, 3-methylene-4-(1,2-propadienyl)-	9.48	0.33
Benzene, 1,1'-(1-ethenyl-1,3-propanediyl)bis-	6.73	0.45	7-Ethylidenebicyclo[4.2.1]nona-2,4-diene	9.66	0.24
Benzene, propyl-	6.86	0.75	Cyclooctene, 3-(1-methylethenyl)-	9.73	0.42
D-Limonene	6.94	1.18	Bicyclo[2.2.1]heptane, 2,2-dimethyl-3-methylene	9.86	0.22
Benzene, 1-ethyl-4-methyl-	6.99	0.67	Cyclopropylphenylmethane	10.26	0.37
Benzene, 1-ethyl-3-methyl-	7.04	1.15	Dodecane	10.73	0.41
Aniline	7.23	0.93	5H-Benzocycloheptene,6,7,8,9-tetrahydro-	11.21	0.30
Alpha Methylstyrene	7.34	1.81	Bicyclo[6.4.0]dodeca-9,11-diene	11.66	0.51
p-Cymene	8.06	3.46	Tridecane	12.18	0.62
D-Limonene	8.16	10.21	8,9-Dimethylbicyclo[4.4.1]undeca-2,4,8-triene	13.11	0.52
Indane	8.25	0.46	Tetramethylbicyclo[7.2.0]undeca-2,6-diene	13.17	0.53
Benzene, 1-propynyl-	8.41	0.43	Tetradecane	13.54	1.37
Benzene, 1-methyl-2-propyl-	8.46	0.36	Cyclohexene, 4-(2-bromoethyl)-	13.88	1.24
Benzeneacetaldehyde, .alpha.-methyl-	8.71	0.16	Valerena-4,7(11)-diene	13.96	0.73
p-Cymene	8.90	0.41	Quinoline, 2,4-dimethyl-	14.22	2.27
Benzene, 1-methyl-4-(1-methylethenyl)-	9.10	0.75	1-Pentadecene	14.74	0.32
Benzene, 1-methyl-4-(1-methylpropyl)-	9.42	0.32	Pentadecane	14.84	1.43
6,7-Dimethyl-3,5,8,8a-tetrahydro-1H-2-benzopyran	9.58	0.15	1,5-Cyclodecadiene	14.93	0.95
1H-Indene, 2,3-dihydro-5-methyl-	9.91	0.47	Guaia-9,11-diene	15.57	0.31
1H-Indene, 1-methyl-	10.06	1.06	Cetene	15.96	0.60
Benzene, pentyl-	10.14	0.81	2-Bromo dodecane	16.05	0.51
Benzene, 2-ethenyl-1,3,5-trimethyl-	10.46	0.17	3-Heptadecene	17.12	0.25
1H-Indene, 2,3-dihydro-1,2-dimethyl-	10.62	0.50	Heptadecane	17.21	1.12
Naphthalene	10.65	0.59	1-Cyclohexene-1-butanol, 2,6,6-trimethyl-	18.23	0.24
1H-Indene, 2,3-dihydro-1,2-dimethyl-	10.77	0.54	Hexadecane	18.29	0.32
Benzene, 2-ethenyl-1,3,5-trimethyl-	11.12	0.27	1,3,6,10-Cyclotetradecatetraene	18.72	0.48
Benzothiazole	11.26	1.19	Cyclohexane, 1-ethenyl-1-methyl	19.53	0.72
Benzene, 1-cyclopenten-1-yl-	11.40	0.20	Eicosane	20.35	1.54
Benzene, cyclohexyl-	11.55	0.60	Heptane, 1,7-dibromo-	20.46	0.38
Naphthalene, 1,2-dihydro-3-methyl-	11.72	0.49	2-Dodecen-1-yl(-)succinic anhydride	21.29	0.18
1H-Indene, 1,1-dimethyl-	11.79	0.22	Bisnorabieta-5,7,9(10),11,13-pentaene	21.43	0.09
Naphthalene, 1,2-dihydro-3-methyl-	11.84	0.56	Heptadecane	22.20	0.21
1H-Indene, 2,3-dihydro-1,2-dimethyl-	12.01	0.33	Tricosane	23.07	0.38
Naphthalene, 1-methyl-	12.28	1.01	Tetracosane	23.91	0.37
Naphthalene, 2-methyl-	12.52	0.50	Heptacosane	24.72	0.45
Benzene, 1,3,5-trimethyl-2-(1-methylethenyl)-	12.64	0.91	Hexacosane	25.49	0.49
Benzene, 3-cyclohexen-1-yl-	12.77	0.41	Nonacosane	26.23	0.39
Benzene, 1-butyl-4-methoxy-	12.96	0.44	Triacontane	28.54	0.42
1,2,3-Trimethylindene	13.31	1.19	Tetratriacontane	29.50	0.24
Naphthalene, 1,2-dihydro-3,5,8-trimethyl-	13.72	0.65			
Naphthalene, 1,2,3,4,4a,5,6,8a-octahydro-4a,8-dimethyl	13.77	0.42	**Phenolics**		
Naphthalene, 2,7-dimethyl-	14.02	1.14	4-Chloro-3-ethylphenol	13.64	0.61
Alloaromadendrene	14.32	0.78			
4,7-Dimethyl-1,2,3,4,4a,5,6,8a-octahydronaphthalene	14.43	1.46	**Acids**		
Benzene, 1-(1,5-dimethyl-4-hexenyl)-4-methyl-	14.66	0.51	9,12-Octadecadienoic acid	7.41	0.78
Naphthalene, 2,3,6-trimethyl-	15.39	0.91	2-Ethoxy-4-methyl-pent-2-enoic acid	12.90	0.84

Compounds	R.T.	%	Compounds	R.T.	%
Naphthalene, 1,4,6-trimethyl-	15.62	0.32	m-Anisic acid, pent-2-en-4-ynyl ester	16.14	0.25
Alloaromadendrene	15.71	0.19	1H-Thieno[3,4-d]imidazole-4-propanoic acid	16.99	0.63
Alloaromadendrene	15.75	0.61	Octadecanoic acid	21.83	0.23
Benzene, [1-(2,4-cyclopentadien-1-ylidene)ethyl]-	16.22	0.30	Octadecanoic acid, ethyl ester	22.13	0.23
Fluorene, 2,4a-dihydro-	16.27	0.48			
Naphthalene, 1-(1,1-dimethylethyl)-	16.41	0.32	**Aldehydes & Ketones**		
Benzene, 1,1'-(1,3-propanediyl)bis-	16.80	0.52	6-Methyl-5,6,7,8-tetrahydro-2,4-quinazolinedione	17.46	0.63
Benzene, (4,5,5-trimethyl-1,3-cyclopentadien-1-yl)-	17.56	0.39	Pregn-17(20)-en-16-one	18.77	0.27
Benzene, 1,1'-(1,4-butanediyl)bis-	17.95	0.44	Androstan-17-one	19.59	0.31
Naphthalene, 2-(1-cyclopenten-1-yl)-	18.47	0.58			
Retene	22.54	0.25	**Nitrogenates Compounds**		
Phenantrene-9,10(9H,10H)	26.86	0.15	Nicotinonitrile, 1,4-dihydro-1-propyl-	9.27	0.43
			Hexadecanenitrile	19.35	1.00
Aliphatics			Octadecanenitrile	21.35	0.54
Cyclohexene, 4-ethenyl-	4.92	0.52	4-Amino-6-iodo-1-methyl-3-oxo-7-carbonitrile	26.63	0.20
1,3,6-Heptatriene, 2,5,6-trimethyl-	6.67	0.47			
cis-2,6-Dimethyl-2,6-octadiene	7.55	1.42			
7-Methylenebicyclo[4.2.0]octane	7.74	0.65			